Petroleum Science 22 (2025) 3056–3067

Contents lists available at ScienceDirect

Petroleum Science

journal homepage: www.keaipublishing.com/en/journals/petroleum-science

Original Paper

Pressure characterization study in the jet influence zone of riser based on HHT analysis

Zhi-Hang Zheng [a, b], Jun-Nan Ma [c], Zi-Han Yan [a, b, *], Chun-Xi Lu [a, b, **]

[a] College of Chemical Engineering and Environment, China University of Petroleum (Beijing), Beijing, 102249, China
[b] State Key Laboratory of Heavy Oil Processing, China University of Petroleum (Beijing), Beijing, 102249, China
[c] China Nuclear Mining Science and Technology Corporation, Beijing, 101149, China

ARTICLE INFO

Article history:
Received 31 August 2024
Received in revised form
28 February 2025
Accepted 16 April 2025
Available online 16 April 2025

Edited by Min Li

Keywords:
Fluidized bed
Riser
Jet influence zone
Pressure pulsation
Hilbert-Huang transform
Distribution

ABSTRACT

By large-scale cold mold experiments, pressure pulsation signals within the jet influence zone of riser reactor are processed by using Hilbert-Huang analysis (HHT) in this study. Effects of different jet forms and operating conditions on the intrinsic mode function (IMF) energy and Hilbert-Huang spectrum are compared. Results show that the IMF energy and Hilbert-Huang spectrum of pressure pulsation signals show significant differences under the influence of upward and downward jets. Moreover, the change of jet velocity will also lead to significant changes in IMF energy and Hilbert-Huang spectrum. Among them, energy values and energy proportions corresponding to high-frequency pressure pulsations show a good correlation with the jet velocity. On this basis, energy value and energy proportion data in the high frequency range of the original pressure signal are clustered and analyzed by using the K-means clustering algorithm. Based on clustering results, the jet influence zone of riser can be defined into three regions. From partitioning results, it is found that the introduction of downward inclined jets could effectively improve the gas-solid mixing in the feed injection zone of riser.

1. Introduction

As a highly efficient reactor, riser is widely used in some energy utilization processes such as fluidized catalytic cracking, crude oil cracking to olefin, biopharmaceutical, and so on (Du et al., 2021, 2023; Gao et al., 2013; Kakku et al., 2024; Li et al., 2023, 2024; Q. Li et al., 2024; Ma et al., 2022; Magrini et al., 2022; Ren et al., 2020; Wang et al., 2022). For example, in the fluidized catalytic cracking (FCC) process, riser reactor is an important place for the feedstock to generate target products (Zhang et al., 2024). The feed oil typically enters the riser as high-speed jets, so as to contact, mix, and react sufficiently with the pre-lift fluid which carries the catalyst particle. By this way, target products such as gasoline, diesel, and propylene are generated. In the above process, more than 70% of the cracking reaction is finished in the feed injection zone (Chen et al., 2021). Thus, the effect of gas-solid mixing in the jet influence zone will directly affect the yield of target products. For an ideal jet influence zone, the gas-solid phase should contact and mix quickly by obtaining the full atomization of raw material droplets (Rossbach et al., 2020; Singh et al., 2024; Wang et al., 2020). In this regard, researchers have proposed a series of optimization measures, including the optimization of the nozzle structure, reducing the diameter of the feed section, and inserting internal components (Barbieri et al., 2023; Quiroz-Pérez et al., 2016; Zheng et al., 2019). Among them, the downward inclined jet feed is believed to be effective in improving gas-solid mixing (Mauleon and Sigaud, 1989). At the same time, it improves the match between catalyst particles and feed injections (Yan et al., 2016). The extent of the jet influence zone is also reduced considerably. It can be seen that changing the jet to downward inclined is one of effective measures available to improve gas-solid mixing (Yan et al., 2023).

In recent years, some studies on the feed injection zone have focused on the particle concentration distribution and the diffusion process of jets (Nikku et al., 2023; Singh et al., 2024). There are few relevant studies on the pressure pulsation distribution within the feed injection zone. Pressure pulsation is one of the crucial

* Corresponding author.
** Corresponding author.
E-mail addresses: yzh@cup.edu.cn (Z.-H. Yan), lcx725@sina.com (C.-X. Lu).
Peer review under the responsibility of China University of Petroleum (Beijing).

https://doi.org/10.1016/j.petsci.2025.04.015

parameters in fluidized bed testing and could reflect the hydrodynamic behavior of fluidized beds effectively. Factors affecting the pressure pulsation signal are complex. It is mainly affected by the nature of the fluidized medium and particle properties. In addition, the geometric characteristics of the fluidized bed and operating conditions could have further effects (Jin et al., 2024; Lian et al., 2022). With the characteristics of rich information, easy detection, and high data accuracy, pressure pulsation is of great significance for the in-depth study of gas-solid two-phase flow. Therefore, more and more analysis methods have been proposed and applied to the analysis of fluidized bed pressure pulsation signals. In general, analysis methods of fluidized bed pressure pulsation are in three categories: time domain analysis, frequency domain analysis, and chaos analysis. Among them, signal analysis methods such as Fourier transform, wavelet analysis and power spectrum analysis have been more mature, which have gained certain recognition in the industry (Bai et al., 2022; Cheng et al., 2024; Gu et al., 2020; Vaidheeswaran and Rowan, 2021; Varghese et al., 2024; Wu and He, 2022; Zhang et al., 2020a, 2020b). For instance, the Fourier spectral analysis is used to analyze pressure pulsations in the riser and proposed that gas flow rate fluctuations and particle clustering are main sources of pressure pulsations (John et al., 1999). The wavelet analysis is used to identify and investigate kinetic properties of pressure-induced bubbles in a fluidized bed (Zhang et al., 2020a, 2020b). Further, the connection between wavelet energy and bubble size is established. By means of power spectrum analysis, the pressure pulsation signal is analyzed in a two-dimensional spout-fluid bed (Zhong and Zhang, 2005). Results show that the frequency of pressure pulsations is related to operating conditions. The main frequency of pressure pulsation can be used to identify the fluidized bed type. However, the above methods have their own certain shortcomings. For example, both the Fourier transform and its derived methods are limited by Heisenberg's immeasurability principle. The resulting power spectrum is ambiguous in time if the frequency is accurate, and ambiguous in frequency if the time is accurate (Lu and Ren, 2023). Wavelet analysis requires pre-selected basis functions and decomposition layers (Zhang et al., 2024). Power spectral analysis has disadvantages of poor variance performance, low resolution, and side flap leakage (Singh et al., 2023).

Besides the above methods, the Hilbert-Huang Transform (HHT) provides a new way for the fluidized bed pressure pulsation signal analysis (Huang et al., 1998). With advantages of being fully adaptive and not subject to Heisenberg's inaccuracy principle, it has an excellent ability to handle non-linear and non-stationary signals (Mei et al., 2024). The HHT analysis can divide the original signal into several Intrinsic Mode Functions (IMFs), according to the characteristic of original signal. The adaptive decomposition process is conducive to the analysis of complex nonlinear signals. Obtained IMFs represent oscillation modes of the original signal under a certain time scale. Each IMF has practical physical significance. In addition, the Hilbert spectrum can provide high-resolution time-frequency information. It can display the instantaneous frequency variation trajectories and energy distributions of all IMFs (Barbosa de Souza et al., 2022; Indragandhi et al., 2024; Matthew et al., 2024; Zhang et al., 2019). However, the HHT also has some unresolved disadvantages. For instance, there is data loss caused by the end effect, and the computational efficiency is low. Nevertheless, with the update of algorithms and the development of computing power, the negative impact brought by above-mentioned disadvantages has been somewhat alleviated (Arslan and Karhan, 2022; Cui et al., 2023; Wei et al., 2021). As a result, researchers have started to attempt to apply the HHT to the analysis of fluidized beds (Lungu et al., 2019). In their study, standardization of four fluidized bed flow patterns is achieved using Hilbert spectral analysis. Results from HHT analysis are in good agreement with the results obtained by other analyses. The pressure pulsation characteristic is investigated in high-pressure fluidized beds (Lu et al., 2013). Results obtained from the HHT analysis effectively reflect the relationship between the energy characteristics of the pressure signal and the flow pattern. The energy index is proposed as an identification of the flow type in a high-pressure fluidized bed.

In the feed section of riser, the gas-solid mixing process is more complicated due to the influence of multiple jets. Conventional signal analysis methods are hardly applicable to analyze the composition of pressure pulsations in this region. The HHT analysis method features strong adaptability and high resolution. It has significant advantages in the analysis of complex signals. Therefore, this paper applies the Hilbert-Huang Transform to analyze pressure pulsation signals in the jet influence zone of riser for the first time. Especially, it is used to analyze the influence of different jet forms on the composition of pressure pulsations. In addition, it is found that the high-frequency pressure pulsation facilitates the promotion of gas-solid mixing (Shah et al., 2017). According to the result of HHT analysis, it is expected to obtain the effect of jet form on the gas-solid mixing. Furthermore, it is anticipated to obtain the relationship between the gas-solid mixing effect and operating conditions. Therefore, this paper focuses on the effect of different forms of jets on the pressure pulsation characteristics in the jet influence zone by using HHT analysis. Based on analysis results, it is proposed that the high-frequency Intrinsic Mode Function is an important indicator for characterizing the gas-solid mixing effect. High-frequency range energies of IMFs within the jet influence zone are clustered by the K-means algorithm. Based on clustering results, the enhancement effect of different jet forms on the gas-solid mixing process is schematically plotted. Compared with relatively complex testing techniques like optical fiber probes, conclusions of this paper can provide an accurate and convenient method for characterizing the gas-solid mixing effect.

2. Experiments

2.1. Experimental setup and measurements

To investigate the pressure pulsation characteristics in the mixing process of jets with pre-lifting fluids in riser, a large-scale cold mold experimental device was built, as shown in Fig. 1. The riser is 0.194 m in inner diameter and 14 m in total height. The

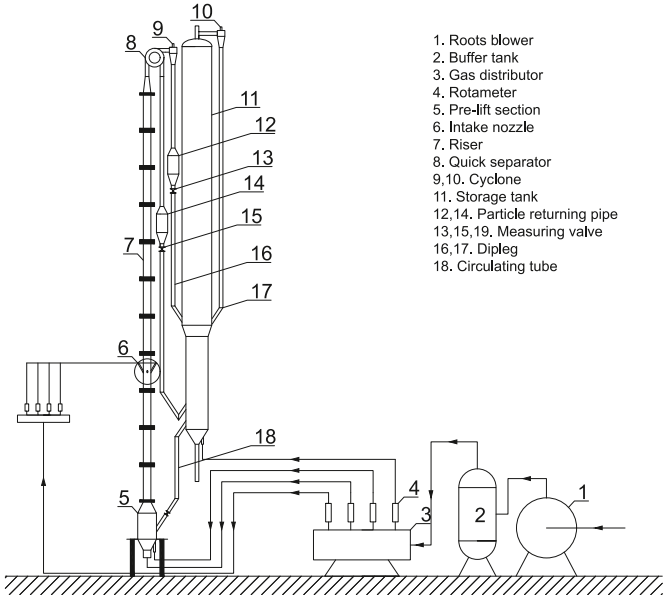

Fig. 1. Experimental setup.

feed injection zone is made of Q235 steel and the rest of the unit is made of plexiglass. Two feeding sections of upward and downward inclined jets used in this experiment are shown in Fig. 2. For each structure, there are four nozzles distributed along the circumference uniformly. For both upward and downward nozzles, angles between the jet and the riser axis are 30°. The fluidized gas used in the experiment is provided by Roots blower 1. The fluidizing gas is divided into four paths and then enters the experimental device after passing through the gas distributor 3. Among them, the first path and the second path enter the bottom of riser 7 respectively and serve as the pre-lift gas and the annular gap fluidized gas for the riser 7. The third path is divided into four streams after secondary distribution to simulate jets. The last path enters the bottom of storage tank and serves as the fluidized gas. After particles enter the pre-lift section 5, the fluidized gas makes them move upward. Then, the pre-lift flow contacts and mixes with jets in the feed injection zone. And the multiphase fluid separates after reaching the end of riser 7. Most of particles are recycled back to the storage tank 11. Particles remaining in the fluidized gas return to the storage tank 11 after being separated by the cyclone separator. Finally, particles return from the storage tank to the pre-lift section 5, completing the entire cycle process.

The measurement system consists of a computer, a data collector, and a differential pressure transducer (CGYL-300B) with a range of 0–20 kPa and a measurement accuracy of 0.001 kPa. The sampling frequency in this experiment is 100 Hz and the sampling time is 100 s. Each group of data was measured three times to eliminate the impact of random errors on experimental results. Positions of axial measurement points for pressure pulsation are set up according to the development stage of jets, as shown in Fig. 3. Set the nozzle inlet cross section as the height of H_0 and set the measurement cross section as the height of H. When the jet is inclined upward, the axial measurement cross sections are $H - H_0 = -0.194$, 0.097, 0.194, 0.388, 0.679, 1.067 m. When the jet is inclined downward, the axial measurement cross sections are $H - H_0 = -0.388$, -0.194, -0.097, 0.097, 0.194, 0.388 m. Positions of radial measurement points for pressure pulsation are shown in Fig. 4. Set the distance between the radial measurement point and the center of riser as r. And set the radius of riser as R. Six radial measurement points are arranged on each measurement section as dimensionless radial position $r/R = 0$, 0.25, 0.5, 0.7, 0.8, 0.95.

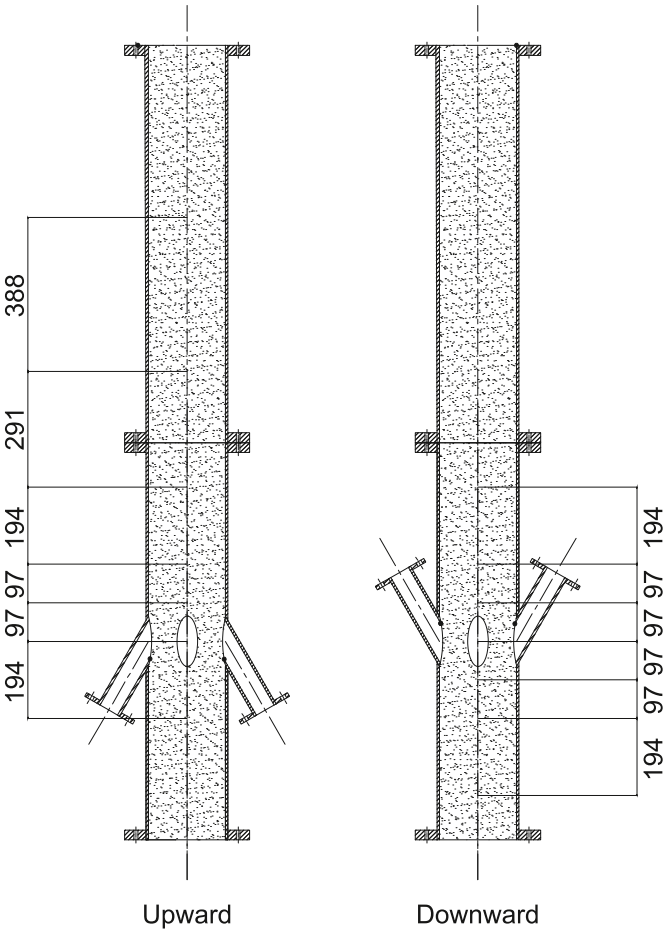

Fig. 3. Sketch of axial measurement points for pressure pulsation (Unit: mm).

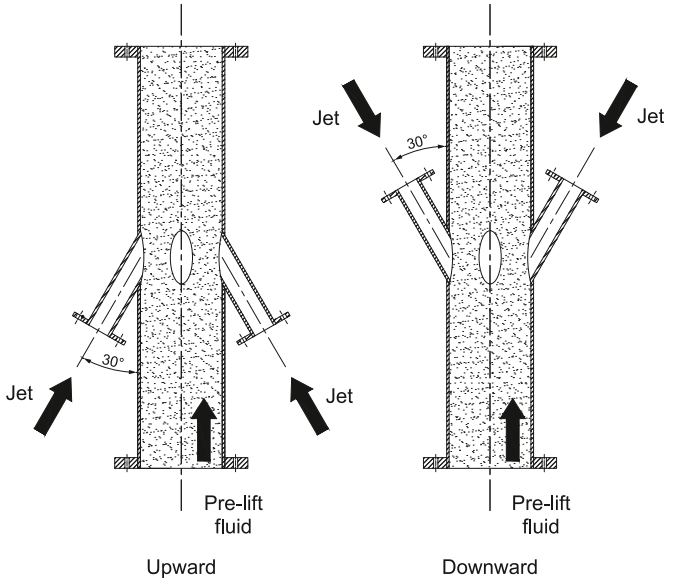

Fig. 2. Sketch of the feeding section with different jet forms.

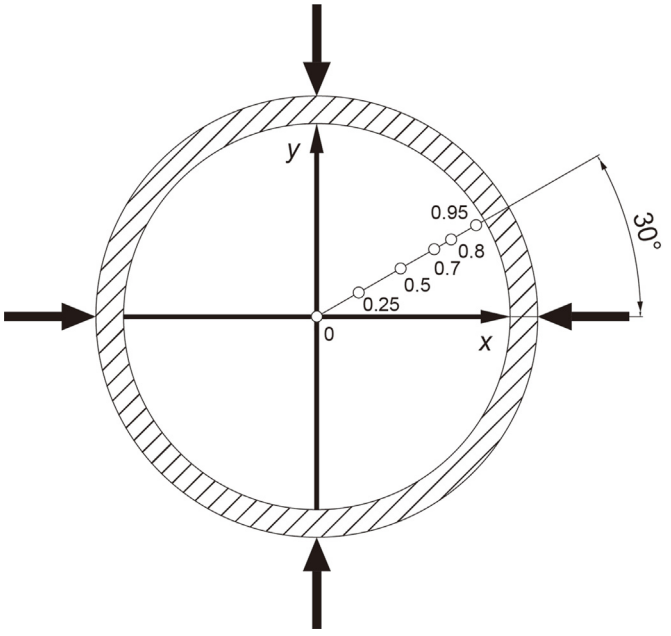

Fig. 4. Sketch of radial measurement points for pressure pulsation.

2.2. Materials and operating conditions

Particles used are FCC equilibrium catalysts. Physical properties of particles are shown in Table 1. In real industrial production, the raw oil will evaporate in a very short time (usually less than 0.2 s (Yan et al., 2023)) after entering the riser, so room-temperature air is used to simulate the pre-lifting gas and nozzle jets in the riser.

Corresponding operating conditions are selected using the FCC process as an example. In the experiments, the pre-lift velocity U_r is set to be 3.5 m/s, the jet velocity U_j at the nozzle exit ranges from 41.8 to 78.5 m/s, and the solid flux G_s is set to be 65 kg/(m^2·s).

3. Analysis method

3.1. Hilbert-Huang transform

The HHT transform (HHT) can be used to deal with non-linear and non-smooth signals. It consists of two main steps: the empirical modal decomposition (EMD) and the Hilbert transform (HT) (Zhang et al., 2023). The raw signal is decomposed by EMD to obtain several IMFs and a residual. Then the Hilbert transform could be applied to each IMF to obtain its instantaneous amplitude and instantaneous phase. The instantaneous frequency of the original signal is obtained by calculation. The integration of obtained results yields the Hilbert-Huang spectrum.

The most remarkable feature of EMD is that it overcomes the problem of lack of the basic functions adaptivity. IMFs after EMD decomposition have the following characteristics:

(1) Within the data segment, the number of extreme points and the number of points past zero must be equal or differ by at most one.
(2) At any moment in time, the average of the upper envelope formed by the local maxima and the lower envelope formed by the local minima is zero. That is, the upper and lower envelopes are locally symmetric concerning the time axis.

EMD decomposition processes the original signal $x(t)$ into several intrinsic mode functions (IMFs), $c_i(t)$ (i = 1, 2, …, n), and a residual, $r_n(t)$. The result is,

$$x(t) = \sum_{i=1}^{n} c_i(t) + r_n(t) \tag{1}$$

where $x(t)$ is the original signal, $c_i(t)$ is intrinsic mode functions, $r_n(t)$ is residuals, n is the number of IMFs and t is the time.

Hilbert transform for each IMF, denoted $y_i(t)$,

$$y_i(t) = \frac{P}{\pi}\int_{-\infty}^{\infty} \frac{c_i(t')}{t-t'}\mathrm{d}t' \tag{2}$$

where $y_i(t)$ is the complex representation of the IMF and P is the Cauchy principal value.

The analytic signal $z_i(t)$ is expressed as

$$z_i(t) = c_i(t) + jy_i(t) = a_i(t)e^{j\phi_i(t)} \tag{3}$$

where $a_i(t)$ is the amplitude and $\phi_i(t)$ is the phase angle. They are defined as,

$$a_i(t) = \sqrt{c_i^2(t) + y_i^2(t)} \tag{4}$$

$$\phi_i(t) = \arctan\left[\frac{y_i(t)}{c_i(t)}\right] \tag{5}$$

The instantaneous frequency, $f_i(t)$, is the derivative of $\phi_i(t)$ concerning time and it can be expressed as,

$$f_i(t) = \frac{1}{2\pi}\frac{\mathrm{d}\phi_i(t)}{\mathrm{d}t} \tag{6}$$

Based on the frequency and amplitude of each IMF, the original signal can be represented as,

$$x(t) = \mathrm{Re}\left[\sum_{i=1}^{n} a_i(t)e^{2\pi j\int f_i(t)\mathrm{d}t}\right] \tag{7}$$

The energy value of each IMF is the mean square value of its amplitude. However, because of the endpoint effect in the HHT analysis, it is necessary to round off signals acquired in the first 10 s and the last 10 s. So, the IMF energy value E_i can be expressed as,

$$E_i = \frac{\int_0^{8000} |c_i(t)|^2\mathrm{d}t}{8000} \tag{8}$$

The total energy E of the original signal can be expressed as,

$$E = \sum_{i=1}^{n} E_i \tag{9}$$

The proportion of total energy accounted for by each part of the IMF energy can be expressed as,

$$P_i = \frac{E_i}{E} \tag{10}$$

It is worth mentioning that jets make the denoising work of original signals extremely complicated. For the purpose of protecting data integrity, pressure signals were not subjected to denoising processing. However, as can be seen from Section 4.1, the energy proportion of the IMF1 frequency band where the noise is located is close to 0. It can be concluded that the noise has not affected the accuracy of the conclusions in this paper.

3.2. K-means cluster

The core objective of K-means is to divide a given dataset into K clusters and give the centroid corresponding to determine their centroids (Y. Li et al., 2024). The algorithm starts by randomly selecting K elements from the original data as the center of each subset. Distances from remaining elements to each center are calculated separately and generalized to the nearest subset. Based on clustering results, continue to iterate until results of the

Table 1
The physical properties of particles.

Mean particle size, μm	Particle size range, μm	Bulk density, kg/m^3	Particle density, kg/m^3
70	30–90	870	1440

clustering no longer change (Miao et al., 2023). The process is as follows:

(1) Divide the original data x_i ($i = 1, 2, \ldots, n$) into k clusters.
(2) Select k initial clustering centers C_k.
(3) Assign the original data x_i to the clustering center C_j ($1 \leq j \leq k$) based on the shortest distance principle. The calculation process is as follows,

$$\|x_i - C_j\| = \min_{1<l<k} \|x_i - C_l\| \tag{11}$$

(4) The formula for regulating the center position of clusters is as follows,

$$C_j = [C_{j1}, C_{j2}, \ldots, C_{jN}]^{\mathrm{T}} \tag{12}$$

$$C_{jp} = \frac{1}{N} \sum_{x \in S_j} x (j = 1, 2, \ldots, k) \tag{13}$$

where p is the number of clusters; N is the amount of data in the jth clustering domain S_j.

(5) If the position of the clustering center stops changing, the calculation stops. Otherwise, continue with step (3).

4. Results and discussion

4.1. Influence of jet forms

The pressure pulsation data of a measurement point under selected experimental conditions is chosen as an example. The EMD decomposition of original signal is performed to obtain multiple IMFs and residuals as shown in Fig. 5. Each IMF will then be processed with the Hilbert transform. Due to endpoint effects, the first 10 s and the last 10 s of processing results need to be rounded off. The final Hilbert spectrogram obtained is shown in Fig. 6. The cloud-scale indicates the amplitude of the original signal.

Similarly, Hilbert spectrograms of target measurement points within the jet influence zone are obtained for an operating condition of $U_r = 3.5$ m/s, $U_j = 41.8$ m/s, $G_s = 65$ kg/(m^2·s).

Typical locations of the mixing process between the jet and the pre-lift fluid are selected for discussion. When the jet is inclined upward, the cross section of $H - H_0 = 0.679$ m is selected; when the jet is inclined downward, the cross section of $H - H_0 = -0.194$ m is selected. Both cross sections are in the main mixing region of the jet influence zone.

Fig. 7 shows the energy proportion and HHT spectra of IMFs at typical positions when the jet is inclined upward. It can be seen that the distribution of the energy proportion of IMFs is similar at $r/R = 0$ and $r/R = 0.8$ in Fig. 7(a). The IMF energy is mainly concentrated in the low-frequency region (bands 8 to 11). From Fig. 7(b) and (c), it is seen that the overall magnitude of IMFs is relatively low, with values less than 0.2. Peaks in amplitude occur mainly within the range of 0–10 Hz. The overall amplitude in the sidewall region ($r/R = 0.8$) is much lower.

Fig. 8 shows the energy proportion and HHT spectra of IMFs at typical positions when the jet is inclined downward. Energy distributions of IMFs at $r/R = 0$ and $r/R = 0.8$ are also similar in Fig. 8(a). However, the IMF energy is mainly concentrated in the high-frequency region (bands 1 to 4). Simultaneously, there are secondary peaks in the low-frequency region (bands 8 to 11). Fig. 8(b) and (c) show that the overall amplitude of IMFs increases significantly compared to the case of upward inclined jet, with a peak

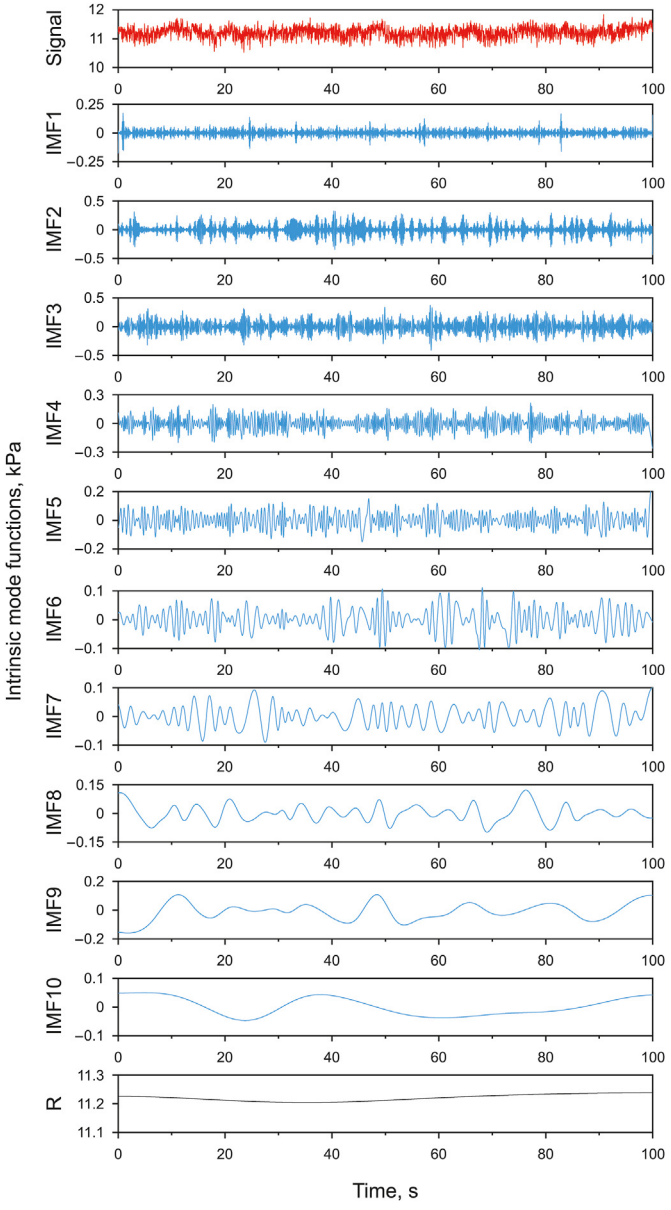

Fig. 5. IMFs component chart.

value of around 0.4 in some bands. Peaks in amplitude occur mainly within the range of 5–20 Hz. In the region near the sidewall of the riser, the IMF amplitude has no significant change compared with the center region.

During the interaction between jets and the multiphase flow, the stronger the intensity of pressure fluctuations generated, the greater the vibration intensity within that region. The intense gas-solid mixing process is conducive to the full contact between the feed gas and catalyst particles. Thus, it could improve the chemical reaction efficiency. In the classical physics theory, the vibration intensity Γ is proportional to the square of the vibration frequency f and the first power of the amplitude A,

$$\Gamma \propto f^2 \cdot A \tag{14}$$

It can be seen from Eq. (14) that the vibration intensity Γ is more sensitive to the vibration frequency. The pressure fluctuation is a manifestation of the vibration of multiphase fluids (Xiao et al.,

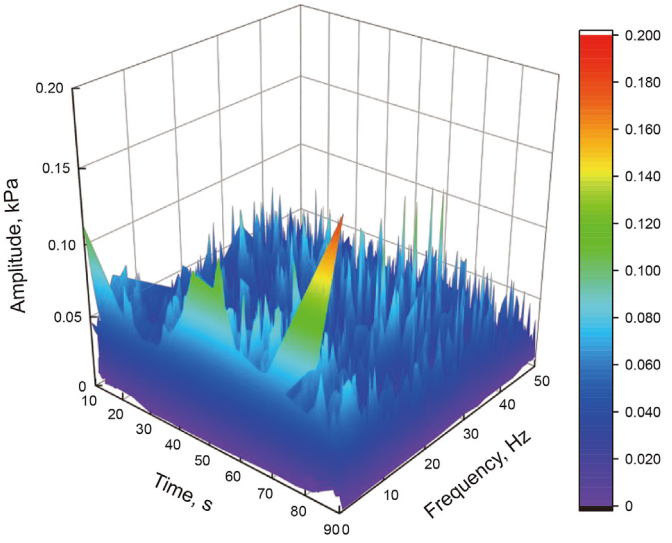

Fig. 6. Hilbert spectrogram.

2024; Yang et al., 2024). Above results show that the gas-solid mixing process is more intense when the jet is inclined downward. This is reflected by larger overall energy values and a higher percentage of total energy for IMFs in the high-frequency range. Therefore, the energy value and the total energy proportion of IMFs in the high-frequency range of the pressure pulsation signal decomposed by the HHT can be used as a standard. In this way, it could evaluate the enhancing effect of the jet on the gas-solid mixing process. The higher the energy value of IMFs in the high-frequency range, the more significant the enhancing effect of pressure fluctuations on the gas-solid mixing process. The greater the proportion of total energy they account for, the fewer low-frequency pulsations are generated during the gas-solid mixing process, indicating a more efficient enhancement.

4.2. Influence of jet velocities

Fig. 9 shows the distribution of high-frequency energy values and energy proportions in the jet influence zone for different jet velocities when the jet is inclined upward. Three typical measurement cross sections are selected according to the development stage of jets. Among them, the cross section of $H - H_0 = 0.194$ m corresponds to the initial stage of jet diffusion, the cross section of $H - H_0 = 0.679$ m corresponds to the intermediate stage of jet diffusion, and the cross section of $H - H_0 = 1.067$ m corresponds to the final stage of jet diffusion. As the jet velocity increases, different cross sections show different results. The value of high-frequency energy decreases with increasing jet velocity in the cross section of $H - H_0 = 0.194$ m. A similar trend is seen for the overall percentage of values. At the cross sections of $H - H_0 = 0.679$, 1.067 m, the overall value of the high-frequency energy and the energy proportion is significantly reduced compared to the $H - H_0 = 0.194$ m cross section. With the increase of the jet velocity, the value of the high-frequency energy and the energy proportion of both cross sections increase. This trend is more pronounced at radial locations of $r/R = 0.5$–0.95. However, the trend of the high-frequency energy proportion is different. The overall energy proportion is lowest at $U_j = 41.8$ m/s, increases to a maximum at $U_j = 64.2$ m/s, and decreases at $U_j = 78.5$ m/s.

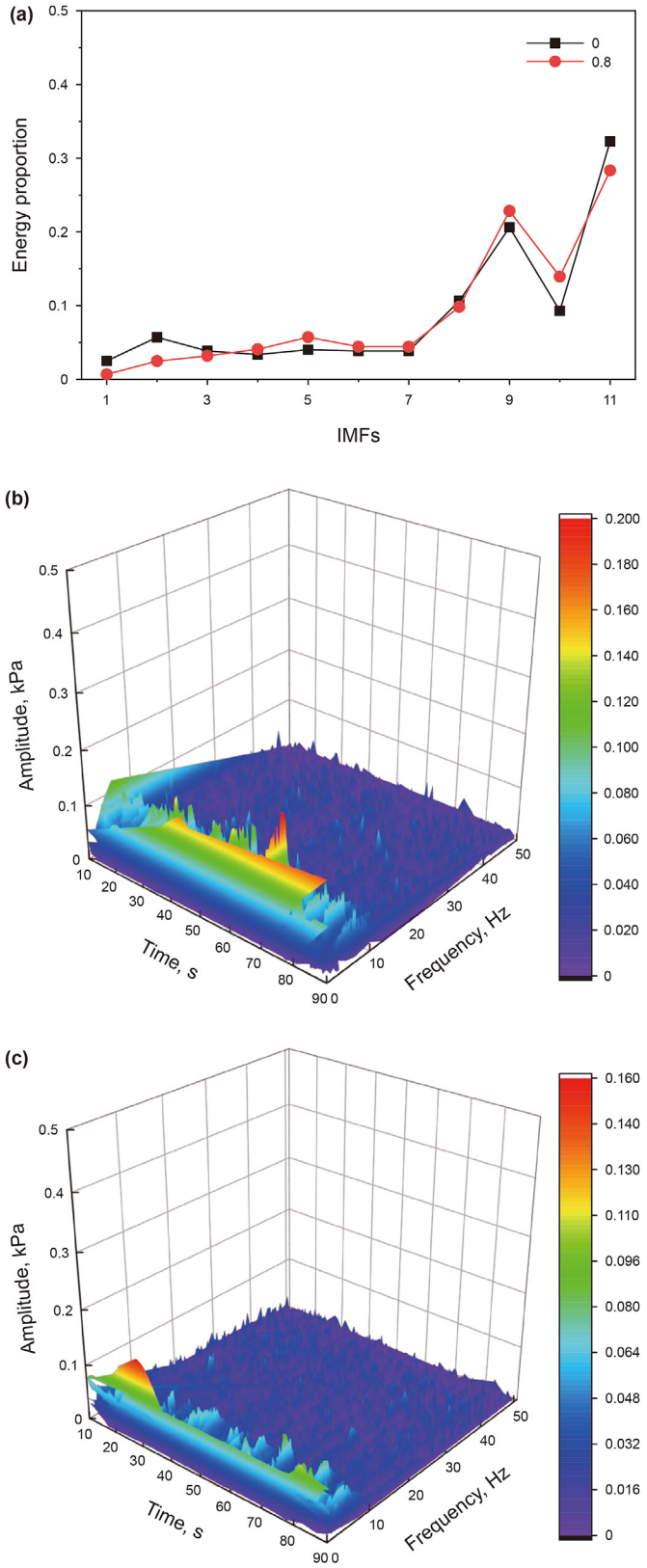

Fig. 7. Energy proportion and HHT spectra of IMFs at typical locations. **(a)** IMFs energy proportion chart; **(b)** HHT spectra at the position of $r/R = 0$; **(c)** HHT spectra at the position of $r/R = 0.8$.

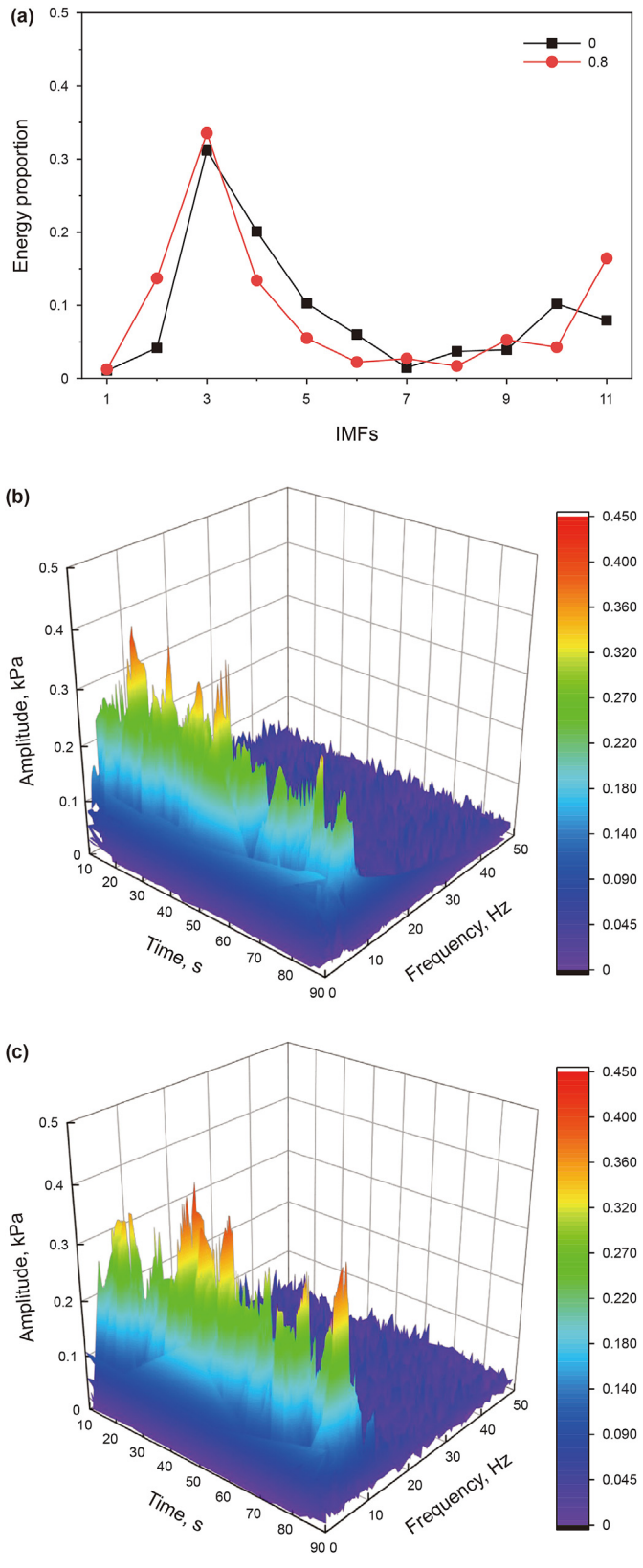

Fig. 8. Energy proportion and HHT spectra of IMFs at typical locations. **(a)** IMFs energy proportion chart; **(b)** HHT spectra at the position of $r/R = 0$; **(c)** HHT spectra at the position of $r/R = 0.8$.

The upward inclined jet will contact and mix with the pre-lift fluid and move upward together after entering the riser. During this process, the jet creates a "secondary flow" directed towards the wall of the riser by the action of the pre-lift flow (Fan et al., 2009; Liu et al., 2021). The secondary flow will entrain catalyst particles and cause them to aggregate toward the sidewall area. Meanwhile, the mainstream of the jet still spreads towards the center of the riser. The above phenomenon leads to a mismatch of the concentration distributions between gas and solids. That is, regions with high jet concentrations have low particle concentrations. On the contrary, regions with low jet concentrations have high particle concentrations. As the jet velocity increases, it decreases the contact efficiency between the jet and solid particles in the region near the inlet cross section (Yan et al., 2018). The intensification of the gas-solid mixing process by the jet is weakened. As a result, corresponding pressure pulsations behave at lower frequencies. This has resulted in a decrease in both high-frequency energy values and energy proportions in the region near the inlet cross section.

In summary, when the jet is tilted upward, the mixing process between the jet and the multiphase flow is not ideal. The increase of jet velocity cannot significantly increase the value of high-frequency energy, but instead leads to a decrease in its percentage after the jet velocity reaches 64.2 m/s. It has a certain negative impact on the gas-solid mixing process. Previous research results have shown that the jet will reach the center region of the $H - H_0 = 0.679$ m cross section and complete the mixing process within $H - H_0 = 1.067$ m (Fan et al., 2002). The mixing process between the jet and the pre-lift flow is still unsatisfactory in the region of $H - H_0 = 0.679 - 1.067$ m (Yan et al., 2018). Within the jet influence zone, time fractions of the cluster phase and the gas phase are quite high. However, the time fraction of dispersed particle phase, which is favorable for gas-solid reactions, is relatively low. Under such conditions, the gas-solid mixing effect will be significantly reduced. Besides, it is difficult to significantly promote the gas-solid mixing in this region by increasing the jet velocity. Instead, it will further lead to an increase in the time fraction of gas phase. The result of ozone decomposition experiment shows that co-current jets will lead to an uneven jet concentration distribution within the jet influence zone. The decomposition rate of ozone during the mixing process is also lower (Yan et al., 2024). The experimental results obtained in this study explain the above experimental conclusions well.

Fig. 10 shows the distribution of high-frequency energy values and energy proportions in the jet influence zone for different jet velocities when the jet is inclined downward. Three typical measurement cross sections are selected according to the development stage of jets. Among them, the cross section of $H - H_0 = -0.194$ m corresponds to the initial stage of jet diffusion, the cross section of $H - H_0 = 0.194$ m corresponds to the intermediate stage of jet diffusion, and the cross section of $H - H_0 = 0.388$ m corresponds to the final stage of jet diffusion. The change in the jet form caused a significant difference in the pressure pulsation within the jet influence zone. When the jet is set to be downward inclined, the overall value of the high-frequency energy in the jet influence zone increases significantly. As the jet velocity increases, the overall value of the high-frequency energy in the jet influence zone increases. In contrast, there is a more pronounced tendency for the sidewall region to increase. The overall energy proportion shows a relatively complex trend. However, the high-frequency energy proportion of different cross sections all reached a maximum at $U_j = 64.2$ m/s.

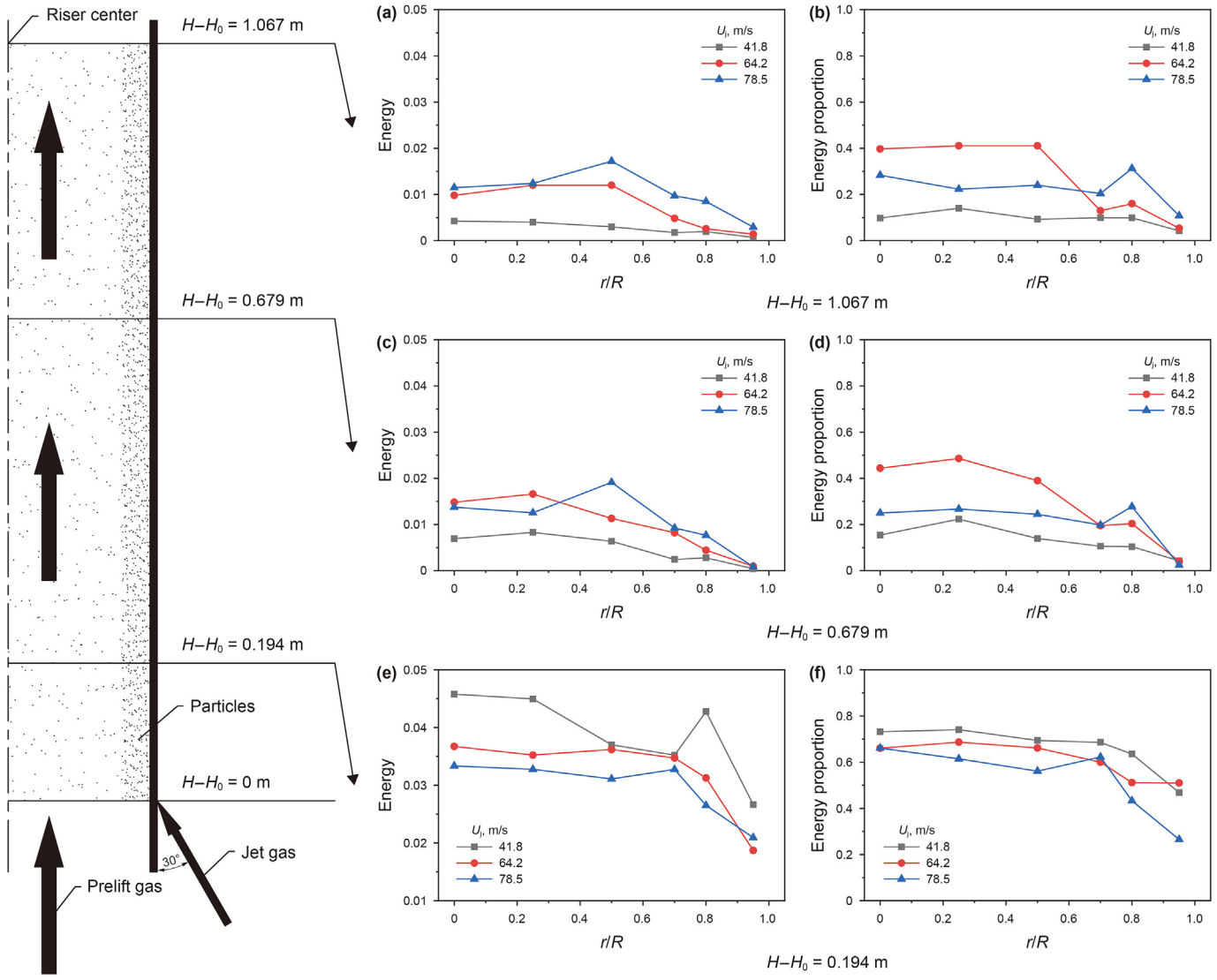

Fig. 9. Distribution of high-frequency energy values and energy proportions in the jet influence zone when the jet is inclined upward. **(a)**, **(c)**, **(e)** The distribution of high-frequency energy values in cross sections of $H - H_0 = 1.067$ m, $H - H_0 = 0.679$ m and $H - H_0 = 0.194$ m; **(b)**, **(d)**, **(f)** the distribution of high-frequency energy proportions in cross sections of $H - H_0 = 1.067$ m, $H - H_0 = 0.679$ m and $H - H_0 = 0.194$ m.

The downward inclined jet will bend upward under the action of the pre-lift flow and mix with it as the jet enters the riser (Yan et al., 2016). During this process, a secondary flow directed toward the center of the riser will be generated. In contrast to the upward inclined jet, the secondary flow will then entrain solid particles to the center area of the riser. At this point, the secondary flow will strengthen the role of jet in regulating the particle concentration distribution in the riser. Increasing jet velocity will increase the "stiffness" of the jet itself. As a result, the velocity of the jet bending upwards decreases, thus expanding the area upstream of the jet influence zone. In this case, more solid particles are entrained into the center of the riser by the jet. The above process leads to a significant increase in high-frequency energy in the center region of the riser during the increase in jet velocity.

After the initial completion of mixing, the multiphase fluid will diffuse towards the sidewall region after passing through the inlet cross section. The jet will coil catalyst particles from the center region to the sidewall region. The mixing of the jet with the pre-lift flow is finally completed thoroughly. Subsequently, the multiphase flow in the riser starts to recover to the typical flow. The increase in jet velocity will result in more catalyst particles being swept up to the sidewall area (Yan et al., 2018). So, the value of the high-frequency energy in the range of $r/R = 0.7–0.95$ increases significantly at the $H - H_0 = 0.194$ m cross section. The high-frequency energy value in the range of $r/R = 0–0.7$ decreases due to the decrease of particle concentration in the center region. However, with the further increase of the jet velocity, the overall effect of the jet on the multiphase fluid within the jet influence zone dominates. As a result, overall values of high-frequency energy in this cross section are increased for jet velocities in the range of 64.2–78.5 m/s. The mixing of the jet with particles is nearly complete after reaching the $H - H_0 = 0.388$ m cross section. Within this cross section, high-frequency energy values show a linear relationship with the jet velocity. It indicates that the increase of the jet velocity will be favorable to promote the gas-solid mixing at the end of the jet influence zone. Judging from results of the optical fiber probe and ozone decomposition, when the jet is inclined downward, the time fraction of gas phase that is unfavorable for the reaction has almost completely disappeared, and the time fraction of cluster phase has also decreased significantly. Instead, the time fraction of

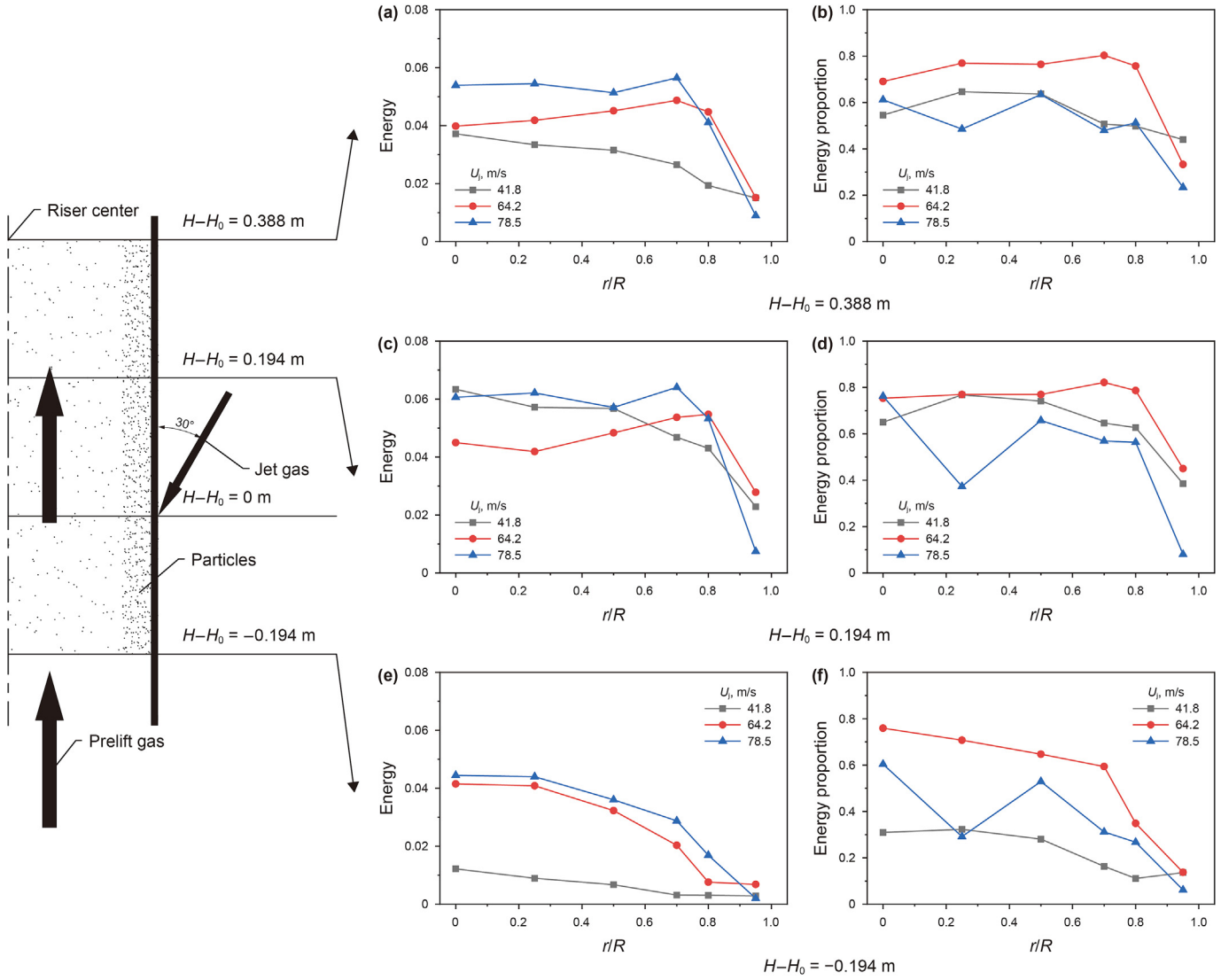

Fig. 10. Distribution of high-frequency energy values and energy proportions in the jet influence zone when the jet is inclined downward. **(a)**, **(c)**, **(e)** The distribution of high-frequency energy values in cross sections of $H - H_0 = 0.388$ m, $H - H_0 = 0.194$ m and $H - H_0 = -0.194$ m; **(b)**, **(d)**, **(f)** the distribution of high-frequency energy proportions in cross sections of $H - H_0 = 0.388$ m, $H - H_0 = 0.194$ m and $H - H_0 = -0.194$ m.

dispersed particle phase, which is conducive to the reaction, has increased significantly (Yan et al., 2018). The rate of ozone decomposition increased significantly under the influence of above factors (Yan et al., 2024). It can be seen that high-frequency pulsation has a significant enhancement effect on gas-solid mixing and reaction processes.

From the distribution trend of the high-frequency energy proportion within the jet influence zone, it can be seen that the overall high-frequency energy proportion is the highest when the jet velocity is 64.2 m/s. This result indicates that appropriately increasing the jet velocity is beneficial to increase the proportion of high-frequency pulsations. However, when the jet velocity is too high, it could lead to the generation of more low and medium-frequency pulsations.

Combining results discussed above, it is concluded that increasing the jet velocity favors the generation of high-frequency pulsations in the jet influence zone. Generally, it is favorable to promote the gas-solid mixing. However, from the experimental results, increasing the jet velocity from 64.2 to 78.5 m/s in most areas does not significantly enhance the high-frequency energy values. Conversely, the excessive jet velocity will significantly reduce the high-frequency energy proportion within the jet influence zone. Resulting pulsations are mostly low and medium-frequency pulsations. It enlarges the region of jet influence zone.

In summary, when the jet is inclined upward, the promotion of the gas-solid mixing within the jet influence zone by the jet is relatively limited. Enhancing the jet velocity can strengthen the gas-solid mixing to some extent just at the end of jet influence zone. However, it can also cause some negative effects on the gas-solid mixing in the region near the inlet cross section. When the jet is inclined downward, the facilitation effect of jet on the gas-solid mixing process within the jet influence zone is obviously increased. It is especially significant in the sidewall region. In addition, appropriately increasing the jet velocity is also beneficial to further enhance the mixing effect. At the same time, the generation of excessive low and medium-frequency pulsations is avoided.

4.3. Generalization of jet reinforcing effects

Multiple operating conditions are selected for the experiment. There are a total of two jet forms for each set of operating

conditions, and data are collected from 36 measurement points each. Take the jet velocity of 64.2 m/s, which optimally promotes the gas-solid mixing effect, as an example. Pressure pulsation signals are processed using HHT analysis to obtain high-frequency energy values and energy proportions for each measurement point. Subsequently, processed results of pressure pulsation signals are clustered using the K-means clustering algorithm. Clustering results show that data points can be successfully categorized into 3 groups as shown in Fig. 11. Data points contained in each group have similar characteristics. For example, data points in Group 1 have lower high-frequency energy values and energy proportions. Data points in Group 3, on the other hand, have higher high-frequency energy values and energy proportions. Therefore, results summarized by the K-means clustering algorithm can better reflect the enhanced effect of the jet on gas-solid mixing.

Based on clustering results, the jet influence zone corresponding to data points in Group 1 can be defined as the "General contact region". The jet influence zone corresponding to Group 2 is defined as the "Enhanced mixing region". The jet influence zone corresponding to Group 3 is defined as the "Efficient mixing region". Thus, the enhancement effect of jet on the gas-solid mixing in the feed injection zone of the riser can be visualized according to the zonal division.

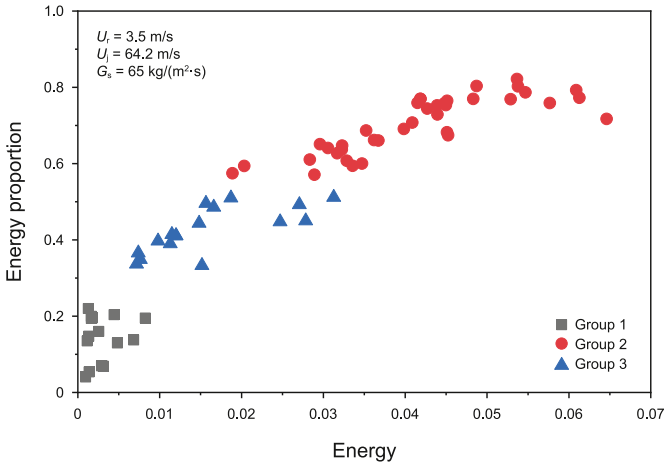

Fig. 11. Scatter plot of clustering results.

According to this method, schematic diagrams of the enhancement effect of different jet forms on the gas-solid mixing process are plotted, as shown in Fig. 12. It is shown that under same operating conditions, when the jet is inclined upwards, the "Efficient mixing region" is mainly concentrated near the downstream of the jet inlet section. As the axial position increases, the enhanced mixing effect of the jet gradually weakens. Generally, the "General contact region" occupies much space within the feed injection zone where the reinforcement is relatively unsatisfactory. When the jet is inclined downward, the space of the "Efficient mixing region" in the jet influence zone accounts for a larger proportion. Meanwhile, it uniformly distributes upstream and downstream of the nozzle inlet. Correspondingly, the percentage of space in the "General contact region" has declined significantly. To make a comparison, it is seen that the downward inclined jet could significantly improve the mixing effect between gas and solid in the riser. Thus, the introduction of counter-current jets is expected to facilitate the reaction performance, especially for reactions that require short contact.

5. Conclusions

In this study, the composition of pressure pulsations within the jet influence zone of riser is investigated using the HHT transform. Results obtained from different jet forms and operating conditions are compared by analyzing the resulting IMFs and HHT spectra. By summarizing the information on values of high-frequency energy and the energy proportion in the jet influence zone, the enhancing effect of the jet on gas-solid mixing is divided into different regions.

Main conclusions of this study are as follows:

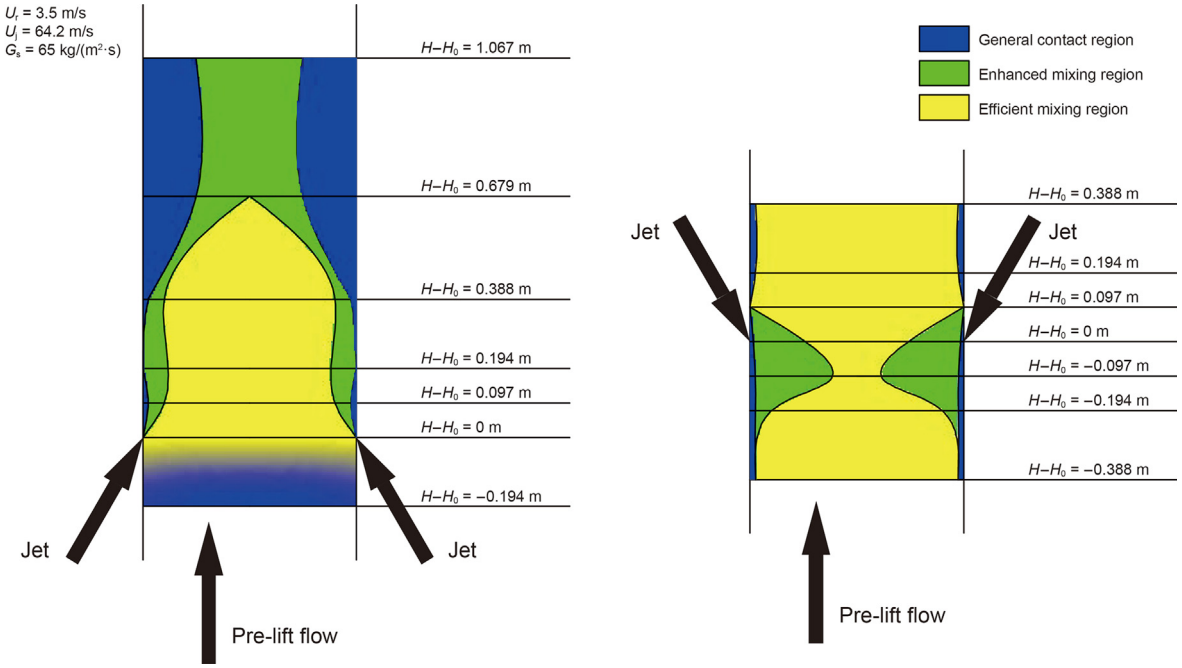

Fig. 12. Schematic diagram of the enhancement effect of different jet forms on the gas-solid mixing.

(1) Compared with the upward inclined jet, pressure signals obtained in the riser with downward inclined jet have a higher intensity of high-frequency pressure pulsations. The axial radial distribution of high-frequency energy values and energy proportions is also more uniform. The strengthening effect of the jet on the gas-solid mixing process is more obvious.
(2) When the jet is inclined upward, as the jet velocity increases, the intensification of the gas-solid mixing process by the jet in the region near the jet inlet cross section is weakened, while in the end region of the jet influence zone, the strengthening effect is enhanced. Generally, in the case of the upward jet, its enhancement on the gas-solid mixing is not satisfactory enough.
(3) When the jet is inclined downward, appropriately increasing the jet velocity could avoid the generation of low and medium-frequency pulsation. Thus, it is conducive to promoting the gas-solid mixing in the jet influence zone. However, excessively high jet velocity will also have a certain negative impact on the mixing process.
(4) Based on the distribution of high-frequency energy values and energy proportions, the jet influence zone is divided into three regions, i.e., General contact region, Enhanced mixing region, and Efficient mixing region. Comparison results show that the percentage of the Efficient mixing region increases significantly when the jet is inclined downward. This indicates that the downward-sloping jet could effectively enhance the gas-solid mixing effects and strengthen the gas-solid contact efficiency. Therefore, for the gas-solid fast reaction process, it is an appropriate method to introduce downward jets for raw material feeding.

CRediT authorship contribution statement

Zhi-Hang Zheng: Writing – original draft, Visualization, Validation, Software, Methodology, Investigation, Formal analysis, Data curation, Conceptualization. **Jun-Nan Ma:** Validation, Investigation, Data curation. **Zi-Han Yan:** Writing – review & editing, Supervision, Resources, Project administration, Methodology, Investigation, Funding acquisition, Formal analysis, Conceptualization. **Chun-Xi Lu:** Writing – review & editing, Supervision, Resources, Project administration, Methodology, Investigation, Funding acquisition, Conceptualization.

Declaration of competing interest

The authors declare that they have no known competing financial interests or personal relationships that could have appeared to influence the work reported in this paper.

Acknowledgments

Funding: This work was sponsored by the National Key Research and Development Program of China (No. 2022YFA1506200), the CNPC Innovation Found (No. 2024DQ02-0203) and the open foundation of State Key Laboratory of Chemical Engineering (No. SKL-ChE-23B02).

References

Arslan, Ö., Karhan, M., 2022. Effect of Hilbert-Huang transform on classification of PCG signals using machine learning. J. King Saud Univ-Com. 34 (10), 9915–9925. https://doi.org/10.1016/j.jksuci.2021.12.019.

Bai, W.J., Chu, D.M., He, Y., 2022. Fluidization dynamic characteristics of carbon nanotube particles in a tapered fluidized bed. Chin. J. Chem. Eng. 44, 321–331. https://doi.org/10.1016/j.cjche.2021.03.006.

Barbosa de Souza, U., Paulo Lemos Escola, J., da, Cunha Brito L., 2022. A survey on Hilbert-Huang transform: evolution, challenges and solutions. Digit. Signal Prossess. 120, 103292. https://doi.org/10.1016/j.dsp.2021.103292.

Barbieri, M.R., Achelis, L., Fritsching, U., 2023. Effect of Y-jet nozzle geometry and operating conditions on spray characteristics and atomizer efficiency. Int. J. Multiphas. Flow 168, 104585. https://doi.org/10.1016/j.ijmultiphaseflow.2023.104585.

Chen, S., Fan, Y.P., Kang, H.Y., et al., 2021. Gas-solid-liquid reactive CFD simulation of an industrial RFCC riser with investigation of feed injection. Chem. Eng. Sci. 242 (5), 116740. https://doi.org/10.1016/j.ces.2021.116740.

Cheng, H., Liu, Z.Y., Li, S., et al., 2024. Machine learning analysis of pressure fluctuations in a gas-solid fluidized bed. Powder Technol. 444, 120065. https://doi.org/10.1016/j.powtec.2024.120065.

Cui, J., Liu, J.W., Ren, G., et al., 2023. An amplitude-nested surrogate model for nonlinear response using double-layer Hilbert–Huang transform. Mech. Syst. Signal Process. 188, 109982. https://doi.org/10.1016/j.ymssp.2022.109982.

Du, W., Ma, L.P., Yang, J., et al., 2021. Experimental and numerical simulation of lignite chemical looping gasification with phosphogypsum as oxygen carrier in a fluidized bed. Chin. J. Chem. Eng. 37, 197–207. https://doi.org/10.1016/j.cjche.2021.01.006.

Du, Y.P., Li, S., Chen, X.P., et al., 2023. A novel methodology to construct compartment models for a circulating fluidized bed riser. Chem. Eng. Sci. 269, 118470. https://doi.org/10.1016/j.ces.2023.118470.

Fan, Y.P., E, C.L., Shi, M.X., et al., 2009. Diffusion of feed spray in fluid catalytic cracker riser. AIChE J. 56 (4), 858–868. https://doi.org/10.1002/aic.12035.

Fan, Y.P., Ye, S., Chao, Z.X., et al., 2002. Gas–solid two-phase flow in FCC riser. AIChE J. 48 (9), 1869–1887. https://doi.org/10.1002/aic.690480905.

Gao, J.S., Tao, X., Wang, G., et al., 2013. Reaction behavior of oil sand in fluidized-bed pyrolysis. Pet. Sci. 10 (4), 562–570. https://doi.org/10.1007/s12182-013-0307-0.

Gu, L.L., Zhang, Y.W., Zhu, S., 2020. Wavelet denoising and nonlinear analysis of solids concentration signal in circulating fluidized bed riser. Particuology 49, 105–116. https://doi.org/10.1016/j.partic.2019.01.005.

Huang, N.E., Shen, Z., Long, S.R., et al., 1998. The empirical mode decomposition and the Hilbert spectrum for nonlinear and non-stationary time series analysis. Proc. R. Soc. A A. 454 (1971), 903–995. https://doi.org/10.1098/rspa.1998.0193.

Indragandhi, V., Kumar, R.S., Saranya, R., 2024. Hilbert-Huang Transform and machine learning based electromechanical analysis of induction machine under power quality disturbances. Results Eng 24, 103075. https://doi.org/10.1016/j.rineng.2024.103075.

Jin, W.X., Gao, J.M., E, C.L., et al., 2024. Pressure fluctuations in a fluidized bed of binary particles with significant differences in particle size. Chem. Eng. Sci. 287, 119704. https://doi.org/10.1016/j.ces.2024.119704.

John, V.D.S., Filip, J., Schouten, J.C., et al., 1999. Fourier analysis of nonlinear pressure fluctuations in gas-solids flow CFB risers-Observing solids structures and gas/article turbulence. Chem. Eng. Sci. 54N (22/24), 5541–5546. https://doi.org/10.1016/S0009-2509(99)00282-1.

Kakku, S., Naidu, S., Chakinala, A.G., et al., 2024. Co-processing of organic fraction from groundnut shell biocrude with VGO in FCC unit to produce petrochemical products. Renew. Energy 224, 120182. https://doi.org/10.1016/j.renene.2024.120182.

Li, Q., Qiu, Q.Z., Cao, H., et al., 2023. Effects of the properties of FCCS on the removing of catalyst particles from FCCS under a DC electrostatic field. Pet. Sci. 20 (3), 1885–1894. https://doi.org/10.1016/j.petsci.2022.11.024.

Li, Q., Yang, H.Z., Yang, C., et al., 2024. Influence of filler characteristics on particle removal in fluid catalytic cracking slurry under an alternating electric field. Pet. Sci. 21 (3), 2102–2111. https://doi.org/10.1016/j.petsci.2023.12.003.

Li, Y., Song, X., Tu, Y.C., et al., 2024. GAPBAS: genetic algorithm-based privacy budget allocation strategy in differential privacy K-means clustering algorithm. Comput. Secur. 139, 103697. https://doi.org/10.1016/j.cose.2023.103697.

Lian, G.Q., Zhong, W.Q., Liu, X.J., 2022. Effects of gas composition and operating pressure on the heat transfer in an oxy-fuel fluidized bed: a CFD–DEM study. Chem. Eng. Sci. 249, 117368. https://doi.org/10.1016/j.ces.2021.117368.

Liu, M., Yao, J., Zhao, Y.L., 2021. The dispersion of particles in turbulent semi-circular duct flows. Pet. Sci. 18 (4), 1240–1255. https://doi.org/10.1016/j.petsci.2021.05.004.

Lu, L., Ren, W.X., 2023. Structural instantaneous frequency identification based on synchrosqueezing fractional Fourier transform. Structures 56, 104914. https://doi.org/10.1016/j.istruc.2023.104914.

Lu, P., Han, D., Jiang, R.X., et al., 2013. Experimental study on flow patterns of high-pressure gas-solid flow and Hilbert-Huang transform based analysis. Exp. Therm. Fluid Sci. 51, 174–182. https://doi.org/10.1016/j.expthermflusci.2013.07.012.

Lungu, M., Siame, J., Sun, J., et al., 2019. Characterization of fluidization regimes and their transition in gas–solid fluidization by Hilbert–Huang transform. Ind. Eng. Chem. Res. 59 (2), 883–896. https://doi.org/10.1021/acs.iecr.9b04364.

Ma, Z.B., Zhang, X.L., Lu, G.J., et al., 2022. Hydrothermal synthesis of zeolitic material from circulating fluidized bed combustion fly ash for the highly efficient removal of lead from aqueous solution. Chin. J. Chem. Eng. 47, 193–205. https://doi.org/10.1016/j.cjche.2021.05.043.

Magrini, K., Olstad, J., Peterson, B., et al., 2022. Feedstock and catalyst impact on bio-oil production and FCC Co-processing to fuels. Biomass Bioenergy 163, 106502. https://doi.org/10.1016/j.biombioe.2022.106502.

Matthew, D.E., Cao, H.R., Shi, J.H., 2024. Advancing chatter detection: harnessing the strength of wavelet synchrosqueezing transform and Hilbert-Huang transform techniques. J. Manuf. Process. 127, 613–630. https://doi.org/10.1016/j.jmapro.2024.07.092.

Mauleon, J.L., Sigaud, J.B., 1989. Process for the catalytic cracking of hydrocarbons in a fluidized bed and their applications. Patent No. 4 883, 583, 28 Nov.

Mei, Y.Z., Wang, Y., Zhang, L.H., et al., 2024. A new method for identifying flow pattern of spouted fluidized bed by coupling Hilbert-Huang transform characteristics of differential pressure signals in different zones. Particuology 89, 67–78. https://doi.org/10.1016/j.partic.2023.10.010.

Miao, D.J., Wang, W.H., Lv, Y.Y., et al., 2023. Research on the classification and control of human factor characteristics of coal mine accidents based on K-Means clustering analysis. Int. J. Ind. Ergon. 97, 103481. https://doi.org/10.1016/j.ergon.2023.103481.

Nikku, M., Myöhänen, K., Ritvanen, J., et al., 2023. Evaluation of mixing of a secondary solid phase in a circulating fluidized bed riser. Chem. Eng. Sci. 269, 118503. https://doi.org/10.1016/j.ces.2023.118503.

Quiroz-Pérez, E., Vázquez-Román, R., Castillo-Borja, F., et al., 2016. A CFD model for the FCC feed injection system. Fuel 186, 100–111. https://doi.org/10.1016/j.fuel.2016.08.067.

Ren, A.X., Wang, T.Y., Tang, T.Q., et al., 2020. Non-spherical particle mixing behaviors by spherical inert particles assisted in a fluidized bed. Pet. Sci. 17 (2), 509–524. https://doi.org/10.1007/s12182-019-00401-4.

Rossbach, V., Padoin, N., Meier, H.F., et al., 2020. Influence of acoustic waves on the solids dispersion in a gas-solid CFB riser: numerical analysis. Powder Technol. 359, 292–304. https://doi.org/10.1016/j.powtec.2019.09.075.

Shah, M.T., Utikar, R.P., Pareek, V.K., 2017. CFD study: effect of pulsating flow on gas–solid hydrodynamics in FCC riser. Particuology 31, 25–34. https://doi.org/10.1016/j.partic.2016.07.002.

Singh, M.N., Khajuria, A., Bajpai, R., et al., 2023. Functional connectivity and power spectral density analysis of EEG signals in trained practitioners of Bhramari pranayama. Biomed. Signal. Proces. 84, 105003. https://doi.org/10.1016/j.bspc.2023.105003.

Singh, R., Marchant, P., Golczynski, S., 2024. Modeling and optimizing gas solid distribution in fluidized beds. Powder Technol. 446, 120145. https://doi.org/10.1016/j.powtec.2024.120145.

Vaidheeswaran, A., Rowan, S., 2021. Chaos and recurrence analyses of pressure signals from bubbling fluidized beds. Chaos Solitons Fractals 142, 110354. https://doi.org/10.1016/j.chaos.2020.110354.

Varghese, M.M., Devan, C.P., Masram, S.M., et al., 2024. Experimental investigation of the behavior of non-spherical particles in a small-scale gas-solid fluidized bed. Flow Meas. Instrum. 95, 102493. https://doi.org/10.1016/j.flowmeasinst.2023.102493.

Wang, B.R., Rui, P.X., Cai, X.H., et al., 2022. Insights into the methanol to olefins (MTO) performance of SAPO-34 under the stripper conditions of fluid catalytic cracking (FCC). Mesoporous Mater. 345, 112244. https://doi.org/10.1016/j.micromeso.2022.112244.

Wang, S.M., Wang, J.R., Song, C., et al., 2020. Numerical investigation on the effects of operating conditions and configuration parameters in industrial risers. Powder Technol. 363, 265–274. https://doi.org/10.1016/j.powtec.2019.12.043.

Wei, B.W., Xie, B., Li, H.K., et al., 2021. An improved Hilbert-Huang transform method for modal parameter identification of a high arch dam. Appl. Math. Model. 91, 297–310. https://doi.org/10.1016/j.apm.2020.09.048.

Wu, G.P., He, Y., 2022. Investigation on gas–solid flow regimes in a novel multistage fluidized bed. Chin. J. Chem. Eng. 46, 21–30. https://doi.org/10.1016/j.cjche.2021.07.014.

Xiao, H., Ma, Y.L., Liu, M.Y., 2024. Diagnoses of flow behaviors in gas-liquid-solid circulating fluidized beds using vibration acceleration signals. Powder Technol. 445, 120070. https://doi.org/10.1016/j.powtec.2024.120070.

Yan, Z.H., Chen, S., Wang, Z., et al., 2016. Distributions of solids holdup and particle velocity in the FCC riser with downward pointed feed injection scheme. Powder Technol. 304, 63–72. https://doi.org/10.1016/j.powtec.2016.03.048.

Yan, Z.H., Fan, Y.P., Bi, X.T., et al., 2018. Dynamic behaviors of feed jets and catalyst particles in FCC feed injection zone. Chem. Eng. Sci. 189, 380–393. https://doi.org/10.1016/j.ces.2017.12.049.

Yan, Z.H., Fan, Y.P., Lu, C.X., et al., 2023. Development and application of counter-current feed injection technology in riser reactors. Can. J. Chem. Eng. 101 (1), 184–194. https://doi.org/10.1002/cjce.24589.

Yan, Z.H., Wang, D.D., Wu, L.N., et al., 2024. Mixing effects of high-speed jets in gas-solid riser and downer reactors. Particuology 92, 196–209. https://doi.org/10.1016/j.partic.2024.05.010.

Yang, X.L., Niu, M.H., Wang, S.B., 2024. Effects of vibration parameters on the drying kinetics of lignite in a vibrated fluidized bed. Fuel 375, 132655. https://doi.org/10.1016/j.fuel.2024.132655.

Zhang, Q., Zhang, G.F., Luo, L., et al., 2024. Improved assessment sensitivity of time-varying cavitation events based on wavelet analysis. Ultrasonics 138, 107227. https://doi.org/10.1016/j.ultras.2023.107227.

Zhang, Q.Y., Cheng, L.M., Li, K., et al., 2024. Experimental study on secondary air mixing along the bed height in a circulating fluidized bed with a multitracer-gas method. Chin. J. Chem. Eng. 70, 54–62. https://doi.org/10.1016/j.cjche.2024.03.003.

Zhang, Y.D., Yang, X.L., Zhu, F.L., et al., 2019. Characteristics of non–linear dynamics and energy transfer in a vibration gas-solid fluidized bed by using Hilbert-Huang transform. Powder Technol. 344, 970–980. https://doi.org/10.1016/j.powtec.2018.12.087.

Zhang, Y.D., Zhang, J.B., Zhao, Y.M., et al., 2020a. Investigations on dynamics of bubble in a 2D vibrated fluidized bed using pressure drop signal and high-speed image analysis. Chem. Eng. J. 395, 125129. https://doi.org/10.1016/j.cej.2020.125129.

Zhang, Y.D., Zhang, X.Y., Zhao, Y.M., et al., 2020b. Bubble growth obtained from pressure fluctuation in vibration separation fluidized bed using wavelet analysis. Adv. Powder Technol. 31 (8), 3287–3296. https://doi.org/10.1016/j.apt.2020.06.018.

Zhang, Z.H., Nie, B.S., Hou, Y.N., 2023. Investigation on energy characteristics of shock wave in rock-breaking tests of high voltage electric pulse based on Hilbert-Huang transform. Energy 282, 128871. https://doi.org/10.1016/j.energy.2023.128871.

Zheng, W.J., Zhang, M., Zhang, Y., et al., 2019. The effect of the secondary air injection on the gas–solid flow characteristics in the circulating fluidized bed. Chem. Eng. Res. Des. 141, 220–228. https://doi.org/10.1016/j.cherd.2018.10.038.

Zhong, W.Q., Zhang, M.Y., 2005. Pressure fluctuation frequency characteristics in a spout-fluid bed by modern ARM power spectrum analysis. Powder Technol. 152 (1), 52–61. https://doi.org/10.1016/j.powtec.2005.01.007.